JOURNAL OF APPLIED ELECTROCHEMISTRY 7 (1977) 485–494

Electrodissolution of nickel sulphide concentrates in ferrous chloride solutions

E. L. GHALI, B. GIRARD, D. V. SUBRAHMANYAM

Centre de Recherche du Moyen Nord, Université du Quebec à Chicoutimi, Canada

Received 3 March 1977

A 3 M ferrous chloride solution of pH 1·5 and operated at 72° C was found suitable to electro-oxidize nickel sulphide concentrates containing the following constituents in wt.%: nickel 20, iron 8, magnesium 10, silicon 8, sulphur 11 and copper 0·83.

The percentages of dissolution for 16 A h at current passed (current density 20–120 mA cm^{-2} with respect to graphite) were in the ranges: Ni 90–70; Cu 70–50 and Mg 20–15. The changes in mol % of the final (mainly elemental) sulphur to initial sulphide–sulphur were in the range of 50 to 25. On the other hand the mole ratio of initial to final iron decreases, and this relates to the precipitation of hydroxides. Corresponding to these changes, the X-ray diffraction patterns detected the presence of elemental sulphur and hydrated oxides of iron and magnesium. The anolyte pH and electrode potential were followed during the electro-oxidation experiments.

Experiments were carried out to establish the feasibility of separating copper from nickel chloride–copper chloride mixtures at 75° C. It was possible to separate copper whose concentration was 5 g l^{-1} or above while that of nickel was 75 g l^{-1}. The cathodic polarization curves for copper, nickel and hydrogen discharge from their individual and binary mixtures were used to predict the conditions required to avoid copper–nickel alloy deposition, and the efficiencies of deposition.

1. Introduction

'Hydrometallurgy' has become an important method of recovering nickel from its oxide ores or pentlandite-rich sulphide concentrates. An economic and pollution-free recovery are the principal objectives behind this approach. Leaching, which is a primary step in this technology, involves the use of acidic or ammoniacal solvents at temperatures above the boiling point and pressures above one atmosphere [1–3]. Majima and Peters [4] reviewed the electrochemical processes involved during the treatment of sulphide minerals. Their review and other publications [5–8] indicate that, until recently, sulphide anodes in their compact form were purified by electrodissolution and subsequent cathodic reduction in acidic sulphate-chloride electrolytes. Recently, the nickel–copper–iron concentrates in the powder form were suspended in electrolytes and were electrolysed. The electrolytes, comprising of alkali metal and alkaline earth chlorides and transition metal chlorides, were operated in a pH range of 0·01–3·9 and a temperature range of 30–80° C [9–11].

A controlled anodic oxidation of the sulphide ores causes the rapid formation of cations in the electrolyte and transformation of the sulphide to elemental sulphur. The elemental sulphur can be recovered by either flotation, or agglomeration or solvent extraction. The coupled chemical reactions will cause the precipitation of hydroxides, oxy-hydroxides and oxides of metals in the solution. The electrochemical reduction gives rise to the deposition of metals in a pure form at the cathode. The use of a diaphragm in the electrolysis cell is indispensable since any introduction of metal sulphides to the cathodic compartment may evolve hydrogen sulphide which is an undesirable product. The anodic and cathodic processes are strongly dependent on the nature of the electrolyte, concentration, pH, temperature, oxygen, agitation and current density. It is expected that the powders in suspension dissolve at accelerated rates because of their large exposed surface. These considerations necessitated studies involving the electrochemical oxidation of nickel–iron–sulphide concentrates in

ferrous chloride solutions at relatively high temperatures in the range 70–80° C. This solution operated at 80° C is reported to accelerate the copper recovery from its sulphide ores containing iron as a constituent [11]. During this process, the ferrous chloride can be partially oxidized to ferric chloride in the anodic compartment. This ferrous–ferric chloride solution can be regenerated for subsequent leaching. It is hoped that this medium will serve as a competitive choice in recovering nickel and iron from the nickel–iron–sulphide concentrates.

Another interesting possibility is the sequential cathodic separation of copper, from mixtures of nickel and iron. It is well known that nickel and iron form mutual alloys even at a nickel to iron ratio of 50 in the sulphate solutions at 53° C (current density = 12·5 mA cm^{-2}) [12]. Hence, it is impractical to separate electrochemically nickel from iron. Utilization of chemical methods like precipitation or solvent extraction in separating nickel from iron may become inevitable. The separation of copper from nickel and iron is quite classical [13] and is practised in certain instances [9–11, 14–16]. However, the pertinent electrochemical information – such as the polarization phenomena involving hydrogen and metal discharge, as well as the minimum concentration of copper, below which it cannot be separated, is lacking with respect to chloride media operated at high temperatures. In order to fill this gap, the feasibility of cathodically separating copper from nickel in their chloride solutions at 75° C was investigated.

It is hoped that the findings on the electro-oxidation of sulphide–silicate concentrates of nickel and iron in ferrous chloride media, in conjunction with the findings on the cathodic separation of copper from nickel can be a positive contribution to the application of electrochemical processes to the hydrometallurgy of nickel.

2. Experimental

2.1. *The electro-oxidation of concentrates*

The nickel sulphide concentrates used in this investigation were subjected to chemical, mineralogical and X-ray (Fig. 6, Table 1) analyses. The chemical analysis was performed on the sample,

Table 1. Analyses of concentrates
(a) *Chemical composition*

Compound	*%*
Ni	20·1
Fe_{total}	8·24
Mg	9·52
S	10·70
SiO_2	17·1
H_2O	14·3
Al_2O_3	0·57
C	1·48
Cu	0.83
CaO	0·28
Co and Cr	traces

(b) *Mineralogical and X-ray analyses* (in Fig. 6).

Phase	*Chemical formula*	*ASTM Card number*
Pentlandite	$(Fe, Ni)_9S_8$	8–90
Heazlewoodite	Ni_3S_2	8–126
Awaruite	Ni_2Fe	–
Millerite*	β-NiS	12–41
Magnetite	Fe_3O_4	11–614
Serpentine	$Mg_3Si_2O_5(OH)_4$	9–444
Brucite†	$Mg(OH)_2$	–

* Found by X-ray analysis.
† Found by mineralogical analysis.

as received. The concentrate-composition in wt.% is: nickel 20·1, iron 8·2, magnesium 9·5, silicon 8·0, sulphur 10·7, carbon 1·48, copper 0·83, calcium oxide 0·28, traces of cobalt and chromium, and water 14·3. The loss on ignition was 26·4%. Mineralogical and X-ray analyses showed the presence of the pentlandite $[Fe, Ni]_9S_8$, heazlewoodite $[Ni_3S_2]$, magnetite $[Fe_3O_4]$, serpentine $[Mg_3Si_2O_5(OH)_4]$ and brucite $[Mg(OH)_2]$ phases. Brucite $[Mg(OH)_2]$ was not detected by X-ray analyses because of its likely presence in small quantities. It was also not possible to determine the minerology of the constituents present in small amounts, i.e., carbon, copper, calcium oxide, cobalt and chromium.

In Fig. 1, the experimental configuration for the electro-oxidation is shown. A rectangular polypropylene cell which could accommodate 600 cc of electrolyte was utilized. The anodic and cathodic compartments were separated by a vinylterylene double diaphragm. The anolyte volume was 250 cc and catholyte volume 350 cc. The plexi-glass cover had provisions for stirrers,

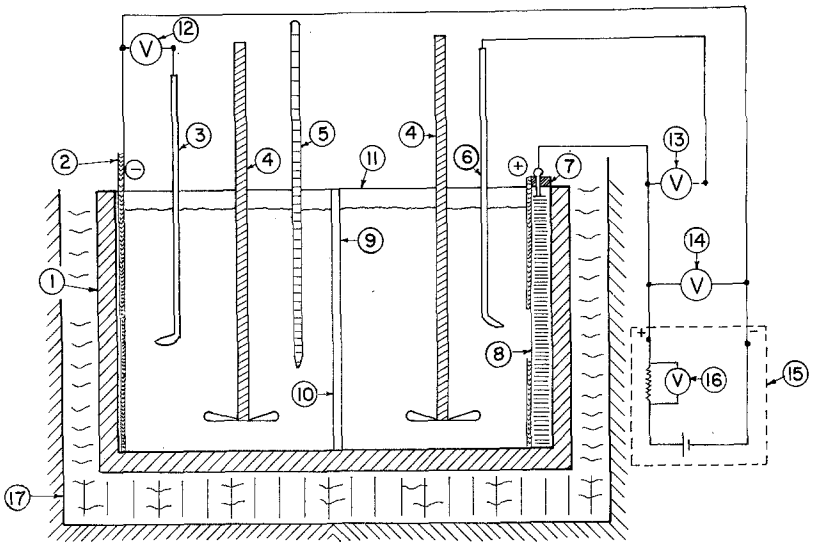

Fig. 1. Experimental arrangement for the electro-oxidation of concentrates.

thermometer, reference and polarizing electrodes. The whole assembly was thermostatted at 72° C. Rectangular graphite (area = 10 cm^2) and copper (area = 40 cm^2) were used as anode and cathode respectively. All of the electro-oxidation as well as the cathodic separation experiments were carried out galvanostatically. The modular mini-potentiostats (made by the Taccusel Co., France) were converted into galvanostats for the cathodic separation experiments. All the electrode potentials were measured with respect to the saturated calomel reference electrode and reported on the same scale.

For each experiment, 50 g of powdered concentrate, 75% of which had a particle size of $< 250\,\mu m$, was used. The concentrate, slurried with 250 cc of 3 M ferrous chloride solution of initial pH 1·5, was electrolysed at 20, 40, 80, 100 and 120 mA cm^{-2}. The quantity of current passed in each experiment was equal to 16 A h. The effect of time corresponding to a certain quantity of current passed, on the percentage dissolution and/or precipitation (normally the ratio of final value to initial value x 100), pH and potentials was also investigated at the current densities 20 and 120 mA cm^{-2}.

After each experiment, the residues were analysed for the changes in the nickel, copper, iron, magnesium, silicon and sulphur contents of the concentrate. The X-ray diffraction patterns were obtained with a Philips diffractometer using unfiltered CuKα radiation to detect the phases before, and after electro-oxidation.

2.2. *Cathodic separation of copper from nickel*

The Cu (II) and Ni (II) chloride solutions used in the present study had the following compositions:

(a) Cu^{2+} = 1·5 and 10 g l^{-1}

(b) Ni^{2+} = 0·5, 1·27 and 3·0 M

(c) Ni^{2+} = 1·27 M, Cu^{2+} = 1·5 and 10 g l^{-1}.

The solutions were purified by activated charcoal treatment and were adjusted to pH 0·8 at 75° C.

The cathode materials were copper, nickel and stainless steel either in the form of strips, discs or rods (mounted in bakelite). An electrode area of 4 cm^2 was used for obtaining the cathodic polar-

ization curves, whereas a 10 cm^2 surface was used for the efficiency and composition measurements. Stainless steel welding rod was used for obtaining the deposition potentials of nickel. A surface area of 0·071 cm^2 was employed for experimental convenience. The electrodes were mechanically polished and subsequently degreased in acetone and chemically etched prior to the electrolysis. The anode was a graphite rod with a geometric area of 20 cm^2.

First, the cathodic polarization curves for the copper and nickel deposition from their respective individual and binary electrolytes were obtained. Also, the hydrogen discharge curves on nickel and copper were obtained in pH 0·8 sodium chloride solutions. At each current density, the potentials were measured in the pseudo-steady-state after 3 min. Then, the current density was made more cathodic. Second, copper was electrodeposited on the stainless steel substrate (area = 5 cm^2) from the copper–nickel chloride mixtures whose compositions were given earlier. The current density, depending on the electrolyte composition, was between 5 and 25 mA cm^{-2}. The deposits were stripped in 1 : 1 nitric acid and were analysed by atomic absorption analysis.

3. Results and discussion

3.1. *The kinetics of dissolution and precipitation*

The influence of the anodic current density and the quantity of current, i.e. influence of time, on the percentages of dissolved nickel, copper, magnesium and silicon, and precipitated sulphur, and iron compounds in 3 M $FeCl_2$ at 72° C are given in Figs. 2 and 3. The current density in each figure is given with respect to the graphite anode.

From Fig. 2, the mean curve drawn for the dissolution of nickel shows that its percentage dissolution decreased with an increase in the current density (quantity of current passed = 16 A h) from 20 mA cm^{-2}. The fluctuations in the data points are within the limits of analytical error. Similarly, the dissolution of copper decreased with increasing current density. On the other hand, the dissolution of magnesium was independent of the current density. The percentages of dissolution were in the ranges: Ni: 90–70; Cu: 70–50; Mg: 20–15. The mole ratio of final elemental sulphur to the initial sulphide sulphur decreased from 50% at 20 mA cm^{-2} to 25% at 120 mA cm^{-2}. Higher anodic current densities can oxidize the elemental sulphur to its sulphate, thus lowering the insoluble sulphur in the residue, and causing the above trend. On the other hand, the mole ratio of initial iron content in the concentrate to the final iron content decreases slightly up to 80 mA cm^{-2} and then increases. Or, conversely, there is a build-up of iron in the residue up to 80 mA cm^{-2} then a decrease afterwards. These observations can also be checked by the solution analyses. Thus at 40 mA cm^{-2}, the following is the solution com-

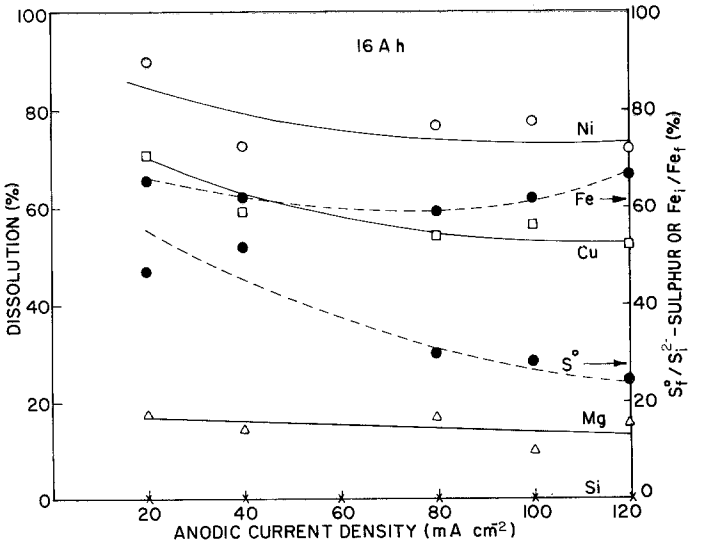

Fig. 2. Influence of the anodic current density on the percentages of dissolution and precipitation. Condition: 3 M $FeCl_2$, 72° C, initial pH 1·5, slurry in anodic compartment and catholyte are stirred (i = initial; f = final).

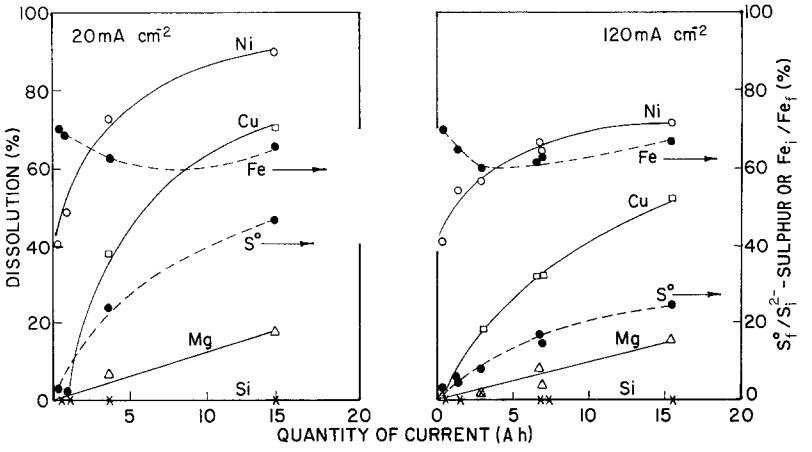

Fig. 3. Influence of the quantity of current on percentages of dissolution and precipitation. Conditions as in Fig. 2 (i = initial; f = final).

position (expressed in $g\,l^{-1}$) after 40 h, or 16 A h of electricity:

Ni: 12·4; Cu: 0·5; Fe: 160; Mg: 1·7.

In particular, the final concentration of iron is less than the initial concentration ($167\,g\,l^{-1}$), indicating the precipitation of iron compounds, e.g. hydroxides. The detailed solution analyses were not carried out due to the unreliability of the data (error = 7 to 30%).

In Fig. 3, the influence of time, i.e. the quantity of current passed, on the concentrate dissolution is given. The early data points correspond to a 30 min interval, or 0·1 A h and 0·6 A h, for the current densities of 20 and 120 mA cm^{-2} respectively. During the early stages, about 40% nickel is dissolved while the other constituents, except iron, are not dissolved. With respect to iron the reciprocal ratio of Fe final/Fe initial is 0·7, confirming the precipitation phenomenon mentioned earlier (Fig. 2). This trend can be caused by the following phenomena:

(a) nickel and iron-based minerals being more active in the EMF series when compared to other minerals: i.e. serpentine, copper;

(b) the chemical attack by Fe^{3+} ion in ferrous chloride being more specific to the nickel and iron (concentration of Fe^{3+} after 2 h = 0·012 M*).

Further attention is being given in an attempt to understand the excessive early-stage dissolution. Further on in Fig. 3, the curves for nickel, copper, iron and sulphur tended to attain maxima while the curve for magnesium was linear. Thus, the constituent phases tend to dissolve by a combination of chemical or electrochemical reactions. The phases which are likely to dissolve electrochemically are: heazlewoodite (Ni_3S_2), awaruite (Ni_2Fe), pentlandite $(Fe, Ni)_9S_8$, and magnetite. The phases which may dissolve chemically are serpentine $Mg_3Si_2O_5(OH)_4$ and brucite $Mg(OH)_2$. Due to the coupled chemical dissolution of constituent phases of the concentrates, the electrochemical dissolution efficiencies could not be estimated accurately. High values were obtained in the beginning. After a passage of 7 A h of current, the efficiencies were around 100% which in turn cannot be due to the electrochemical dissolution alone.

3.2. *Anolyte pH and potentials*

Fig. 4 shows that the anolyte pH became more acidic with time especially during the first 7 A h interval. An initial value of pH 4 corresponds to the instant when the concentrate is added to the anolyte. At this pH, iron hydroxides precipitate out, and a subsequent pH-lowering takes place due to the depletion of OH^- ions in the solution. In Fig. 5, it can be seen that the anode potentials increased from 1·45 to 1·75 V at 20 mA cm^{-2}, and from 2·35 to 2·60 V at 120 mA cm^{-2} at the electrolysis times corresponding to > 0 to 16 A h of current passed. The potential increase as a function of time is not uncommon and such a trend has been reported with the compact matte

* Estimated by EDTA method.

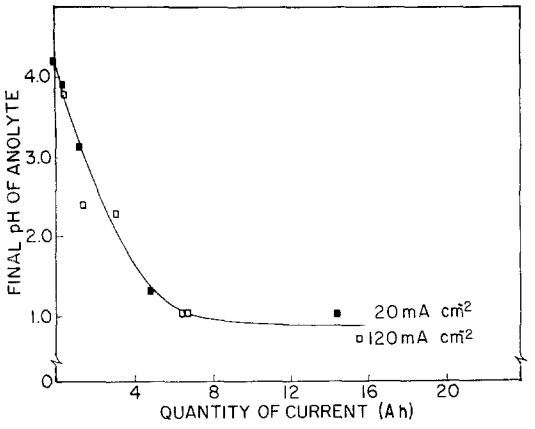

Fig. 4. Quantity of current–final anolyte pH curves. Conditions as in Fig. 3.

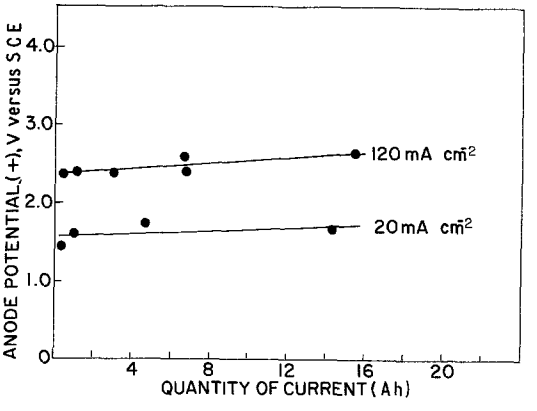

Fig. 5. Quantity of current–anode potential curves. Conditions as in Fig. 4.

anodes containing nickel, copper, iron and sulphur electrolysed in sulphuric acid [5, 17] and sulphate-chloride [18] electrolytes. The potentials reported in the present study, as well by others [5, 17, 18], include ohmic and reaction resistive components. A reduction in slurry density due to the particle dissolution increases the ohmic component whereas the formation of barrier or passivating layers increases the reaction resistive component. Reduction in the slurry density and the formation of barrier or passivating films are detrimental factors in obtaining good yields.

3.3. *Electro-oxidation and phase changes*

Some typical X-ray diffractometer patterns of the concentrate before, and residue after the electro-oxidation are given in Fig. 6. With an increase in the current density as well as time, there is either a reduction in the line intensities or a disappearance of some reflections. This corresponds to the progressive dissolution of the individual constituents. The new lines were assigned to the following new phases:

(a) combination of rhombohedral (ASTM-13-144) and orthorhombic sulphur (ASTM-8-247);

(b) iron sulphate hydroxide, i.e. $3Fe_2O_3.4SO_3.9H_2O$ (ASTM-18-653, 18-515 and 644), α and γ FeOOH (ASTM-3-0249, 17-536 and 5-0499); and

(c) magnesium sulphate chloride hydrate, i.e. $Mg_2Cl_2.SO_4.8H_2O$ (ASTM-20-670).

3.4. *Cathodic separation of copper from nickel*

The cathodic polarization curves for the deposition of copper and nickel from copper (II) chloride, nickel (II) chloride and their mixtures, respectively and for hydrogen evolution in pH 0·8 sodium chloride solutions are shown in the Figs. 7–9. The common features in these figures are that the $Cu^{2+} + 2e \rightarrow Cu$, $Ni^{2+} + 2e \rightarrow Ni$, and $H^+ + e \rightarrow \frac{1}{2}H_2$ reactions are depolarized by an increase in the concentration and at higher temperatures. The polarization curves were quite shallow and hence the precise metal deposition potentials were difficult to obtain. In Fig. 7, it can be seen that there is a considerable concentration polarization for copper deposition when Cu^{2+} in solution is 1 g l^{-1}. The polarization curves for copper and hydrogen reduction intersect at this concentration, thus indicating that co-reduction of hydrogen and deposition of copper is possible at efficiencies below 100%. At $Cu^{2+} = 5$ g l^{-1}, the hydrogen and copper polarization curves are 450 mV apart, indicating that copper deposition at efficiencies close to 100% is possible due to the retarded hydrogen co-discharge. As seen in Fig. 8, the polarization curves for hydrogen discharge at 25° C (curve □) and 75° C (curve ●) lie amidst the nickel discharge curves, indicating that the deposition of nickel will occur at below 100% efficiencies due to the co-reduction of hydrogen ions.

Fig. 9 gives the cathodic polarization curves for the deposition of copper from copper chloride (Cu = 10 g l^{-1}), nickel from nickel chloride (Ni = 1·27 M, □) and their binary mixtures con-

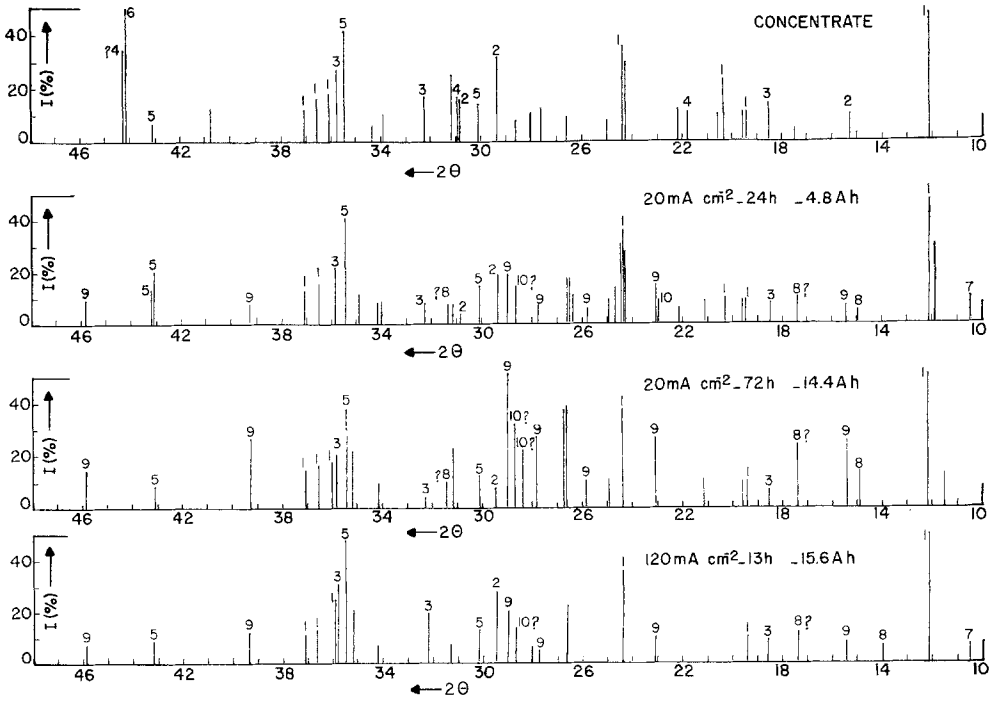

Fig. 6. The X-ray diffractometer patterns of the concentrates. (1) $3\,MgO\,.\,2SiO_2\,.\,2H_2O$-serpentine; (2) $(Fe, Ni)_9S_8$-pentlandite; (3) β-NiS-millerite; (4) Ni_3S_2-heazlewoodite; (5) Fe_3O_4-magnetite; (6) Ni_2Fe-awaruite· (7) $Mg_2Cl_2SO_4\,.\,8H_2O$-magnesium chloride sulphate hydrate; (8) $\frac{1}{2}(3Fe_2O_3\,.\,4SO_3\,.\,9H_2O)$-iron sulphate hydroxide; (9 and 10) Orthorhombic and rhombohedral sulphur respectively.

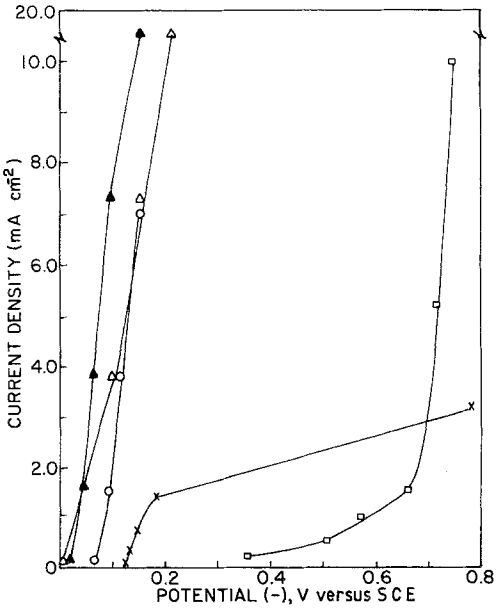

Fig. 7. Cathodic polarization curves in pH 0·8 cupric chloride electrolytes. Temperature is 75° C, unless otherwise stated. Concentration of Cu^{2+} at Cu cathode in $g\,l^{-1}$: × - 1; ○ - 5; △ - 10 (25° C); ▲ - 10; □ - 10 Cl^- as NaCl.

taining 1, 5 and 10 $g\,l^{-1}$ of copper and 1·27 M nickel (*x*-, Δ- and *o*-). In some industrial leaching processes, this concentration of nickel is reached and that is why the above concentration of nickel has been chosen. The polarization curve for hydrogen discharge is also given in this figure. At higher current densities, the curves for nickel, nickel + 1 $g\,l^{-1}$ Cu and hydrogen are closer and thus the deposition of nickel-contaminated copper at low efficiencies will occur.

Table 2 shows the influence of the concentration of copper on copper deposition from a 1·27 M nickel-bearing solution. Copper can be separated without any nickel contamination until the copper concentration in the solution is around 5 $g\,l^{-1}$. The poor efficiency at 1 $g\,l^{-1}$ of Cu in solution is in agreement with the predictions from Fig. 7. Copper deposits at 30% efficiency from a 5 $g\,l^{-1}$ copper-containing electrolyte at 15 mA cm^{-2}. The deposit is coarse, burnished and non-adherent, indicating the attainment of a limiting current density. The cathodic efficiencies under other conditions were around 70%.

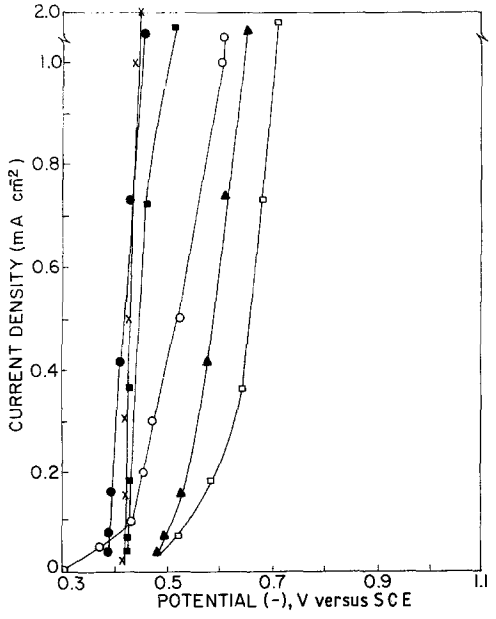

Fig. 8. Cathodic polarization curves in pH 0·8 nickel chloride electrolytes. Temperature is 75° C, unless otherwise stated.

Concentration of Ni^{2+} (M)	*Cathode*
○ - 0·50	Cu
□ - 1·27 (25° C)	S. S.
■ - 1·27	S. S.
X - 3·00	Cu
▲ - 1·27 (25° C) NaCl	Ni
● - 1·27 NaCl	Ni

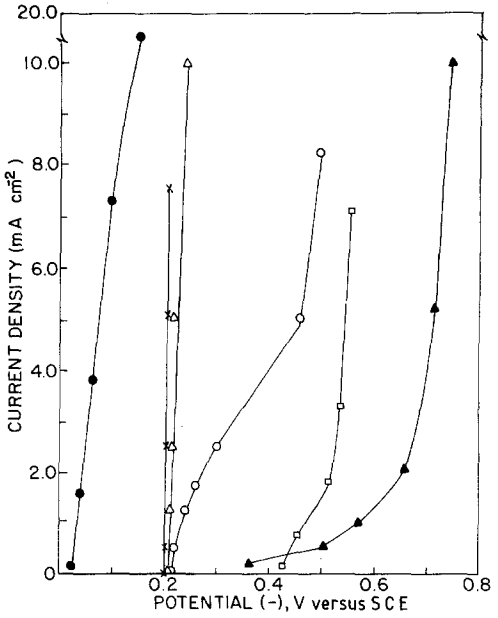

Fig. 9. Cathodic polarization in copper chloride, nickel chloride and their mixtures. Conditions as in Fig. 8.

Concentration	*Cathode*
□ - 1·27 M Ni^{2+}	Ni
○ - 1·27 M + 1 g l^{-1} Cu^{2+}	
△ - 1·27 M + 5 g l^{-1} Cu^{2+}	
X - 1·27 M + 10 g l^{-1} Cu^{2+}	Cu
● - 10 g l^{-1} Cu^{2+}	
▲ - 10 g l^{-1} Cl^- as NaCl	

3.5. *Some critical comments*

The principal constituents of the concentrate and solution undergo a combination of electrochemical and chemical dissolution and/or precipitation reactions as listed below.

3.5.1. Electrochemical reactions

$$FeNiS_2 \text{ (pentlandite)} \rightarrow Fe^{2+} + Ni^{2+} + 2S^0 + 4e \quad (1)$$

$$Ni_3S_2 \text{ (heazlewoodite)} \rightarrow 2\beta\text{-NiS (millerite)} + Ni^{2+} + 2e \quad (2)$$

$$E^0 = +0{\cdot}253\,V$$

Table 2. Influence of copper concentration in solution on the copper in deposit

Concentration of Cu (g l^{-1})	*Current density* (mA cm^{-2})	*% Cu in deposit*	*Efficiency* (%)	*Cathodic potential* (mV)
10	15	100	71	−265
	25	100	69	−290
5	10	100	70	−290
	15*	100	31	−320
1	5	93	11	−310

Ni 1·27 M, 75° C, pH 0·8; unstirred solutions.
* Limiting current density.

$$\beta\text{-NiS} \rightarrow Ni^{2+} + S^0 + 2e \quad E^0 = -0{\cdot}197\,V \quad (3)$$

$$Ni_2Fe \text{ (awaruite)} \rightarrow 2Ni^{2+} + Fe^{2+} + 6e \quad (4)$$

$$2Fe^{2+} + 3H_2O \rightarrow Fe_2O_3 + 6H^+ + 2e \quad E^0 = -0{\cdot}728 \quad (5)$$

$$S + 4H_2O \rightarrow SO_4^{2-} + 8H^+ + 6e \quad E^0 = -0{\cdot}357. \quad (6)$$

3.5.2. Chemical reactions

$$Fe^{3+} \xrightarrow{\text{hydrolysis}} Fe_2O_3 \rightarrow Fe(OH)_3 \quad (7)$$

$$Mg_3Si_2O_5(OH)_4 \text{ (serpentine)} \xrightarrow{Cl^-} MgCl_2. \quad (8)$$

In comparison to the Fe^{2+} ion, the Ni^{2+} ion is stable over a broad range of potentials. The standard potentials given above are at 25° C and are bound to be different at 75° C due to the changes in the standard entropies and partial molal heat capacities of the ions. These changes generally do not alter the preferred incidence of the mentioned reactions. Thus, at anodic potentials between + 1·35 and 2·6 V (Fig. 5) corresponding to the final pHs (Fig. 4), oxides of iron must result from the thermodynamic instability considerations. Moreover, in the above potential interval sulphate ions [19] are expected to be formed (Reaction 6). The detection of iron sulphate hydroxide by X-ray analyses (Fig. 6) and the lowering of the mole percentage of final to initial sulphur (Fig. 2) with an increase in current density support the above predictions.

The hydrolysis of iron as given by Equation 7 appears to be assisted by the possible common ion effects. The solubility products for $Fe(OH)_3$, $Fe(OH)_2$ and $Mg(OH)_2$ are of the order 10^{-36}, 10^{-14}, and 10^{-11} respectively [20]. As the $Mg_3Si_2O_5(OH)_4$ (serpentine) dissolves by Reaction 8, the $[OH^-]$ concentration, i.e. pH, rises, favouring Reaction 7. Thus, in Fig. 10, it can be seen that as the magnesium in the residue decreases due to its solubilization, the iron content in the residue increases due to precipitation. The hydrolysis of ferric ion as well as the formation of blocking layers by Reactions 1–3 and 5 are the causes of diffusion control. Thus, from a practical view-point it is beneficial to electro-oxidize the concentrate at lower current densities of the order of 20 mA cm^{-2} for shorter times, e.g. in the vicinity of 7 A h. Alternatively, repleneshing the concentrate to the initial slurry density would maximize the efficiency of electro-oxidation.

Furthermore, during the electro-oxidation stage itself, copper can be cathodically separated from nickel, iron, magnesium, silicon, as illustrated by the results shown in Figs. 7–9 and Table 2. If copper could be separated successfully from nickel, it can also be separated from the constituents whose redox potentials are more active than that of nickel. The conditions for maximizing copper recovery can be optimized by pH adjustment, agitation (increases the diffusion current), or by cementation of the unrecovered copper in solution by suitable cementing agents, e.g. zinc dust.

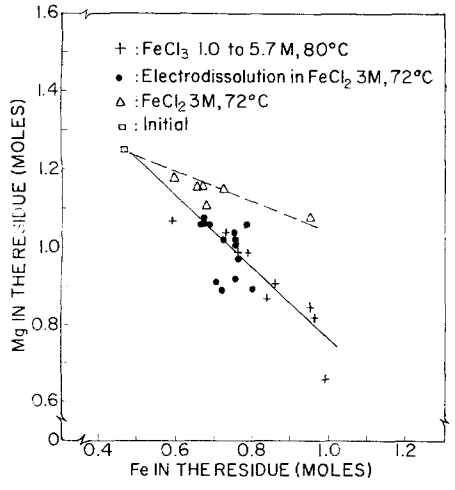

Fig. 10. Relationship between the magnesium and iron during leaching and electro-oxidation.

4. Conclusions

(1) The electro-oxidation process can be applied to nickel sulphide–magnesium silicate concentrates containing nickel, iron, copper and magnesium in 3 M ferrous chloride solution at 72° C.

(2) In view of the diffusion-controlled processes retarding the recovery, a suitable condition is a current density of around 20 mA cm^{-2} or below, which, for the quantity of current around 7 A h, constitutes a suitable condition to recover elemental sulphur, as evidenced by the X-ray diffractometer patterns.

(3) Electro-oxidation affects the dissolution of the metallic phase i.e. awaruite and sulphide phases i.e. heazlewoodite, millerite and pentlandite. The new phases formed during the electro-oxidation were rhombohedral and orthorhombic sulphur, iron sulphate hydroxide, α and γ-FeO.OH and magnesium sulphate chloride hydrate.

(4) Cathodic separation experiments prove that copper can be recovered as cathodic product while the concentrate is being electro-oxidized.

Acknowledgements

The authors thank the Quebec Ministry of Natural Resources for supporting the work, and Yvon Laliberté (Direction of Mineral Economy and Development), Gérard Castonguay and Arpad E. Torma (Mineral Research Center), for encouragement, discussions and the laboratory facilities.

References

[1] J. R. Boldt, 'The Winning of Nickel', Longmans Canada Ltd (1967) pp. 193, 290.
[2] R. F. Blanks, *Austral. Chem. Processing Engng*, **23**, (8) (1970) 19, 21, 23–6.
[3] B. Meddings and D. J. I. Evans, *CIM Bulletin*, **64** (1971) 48.
[4] H. Mijima and E. Peters, *Proc. 8th International Mineral Processing Congress*, Leningrad (1968).
[5] S. Venkatachalam and R. Mallikarjunan, *Inst. Mining and Metallurgy* 77 (1968) C45.
[6] D. M. Chizhikov, L. V. Pliginskaya, E. A. Subbotina, N. V. Skorduli and R. I. Komarova, *Elektrokhimya* 9 (4) (1973) 449.
[7] D. M. Chizhikov and B. Z. Ustinskii, *Izvest. Akad. Nauk S. S. S. R. Otdel. Tekh. Nauk* (1949) 1481; *Chem. Abs.* **45** (1951) 6093b.
[8] L. S. Renzoni and W. V. Barker, U. S. Pat. 2 839 461 (1958).
[9] P. R. Kruesi and D. N. Goens, U. S. Pat. 3 736 238 (1973).
[10] P. R. Kruesi, U. S. Pat. 3 766 026 (1973).
[11] P. R. Kruesi, E. S. Allen and J. L. Lake, *CIM Bulletin* **66** (6) (1973) 81.
[12] A. Brenner, 'Electrodeposition of Alloys', Academic Press, Vol. II (1963) p. 268.
[13] A. I. Vogel, 'Quantitative Inorganic Analysis', John Wiley and Sons Inc. (1961) p. 617.
[14] F. L. Duffield, U. S. Pat. 328 696 (1930).
[15] W. C. Hazen, U. S. Pat. 3 767 543 (1973).
[16] P. R. Kuresi, U. S. Pat. 3 673 061 (1973).
[17] D. M. Chizhikov and B. Z. Ustinskii, *Zhur. Priklad. Khim.* **29** (1956) 1129; *Chem. Abs.* **50** (1956) 16474.
[18] A. A. Bulakh and O. A. Khan, *ibid* **27** (1954) 166; *Chem. Abs.* **48** (1954) 8037.
[19] M. Pourbaix, 'Atlas of Electrochemical Equilibria in Aqueous Solutions', N. A. C. E. (1966).
[20] S. H. Maron and E. H. Prutton, 'Principles of Physical Chemistry', Macmillan, London (1969) p. 461.